Atomic Force Microscopy Study of the Pressure-Dependent Structural and Frictional Properties of *n*-Alkanethiols on Gold

A. Lio,† C. Morant,‡ D. F. Ogletree, and M. Salmeron*

Materials Sciences Division, Lawrence Berkeley National Laboratory, University of California at Berkeley, Berkeley, California 94720

Received: November 14, 1996; In Final Form: April 2, 1997[⊗]

Atomic force microscopy (AFM) has been used to study the effect of pressure on the structural and frictional properties of self-assembled monolayers of *n*-octadecanethiol on Au(111). Sharp microfabricated silicon nitride tips (tip radii 100−300 Å) were used. At low load, the periodicity of the thiol layer is imaged. At higher load, the layer is observed to become disordered. At a critical contact pressure of ∼2.3 GPa, a transition from the thiol overlayer to the Au(111) substrate periodicity is observed in the lattice resolution images. This transition is gradual and reversible. During the transition, frictional forces first increase and then decrease as the tip−sample separation decreases by a distance approximately equivalent to the thickness of the thiol layer.

Introduction

Self-assembled monolayers (SAMs) of alkyl thiols $CH_3(CH_2)_{n-1}SH$ (C_n) on Au(111) have been widely investigated in the past 10 years.[1−4] They are relatively easy to prepare and give well-ordered, close-packed films for $n > 8$. A model based on diffraction and spectroscopy studies[2,3,5,6] had the sulfur atoms adsorbed in 3-fold hollow sites on the Au(111) surface in a $(\sqrt{3} \times \sqrt{3})$R30° unit cell. The alkyl chains were in an *all-trans* conformation and tilted ∼30° from the surface normal. A "c(4 × 2)" superlattice (relative to the $(\sqrt{3} \times \sqrt{3})$R30° structure) has been observed in He diffraction,[4] X-ray diffraction,[7] and scanning tunneling microscopy (STM) studies.[8,9] AFM studies have shown a hexagonal $(\sqrt{3} \times \sqrt{3})$R30° unit cell.[10] More recently, sum frequency generation (SFG) experiments[11] show that the arrangement of S atoms relative to the Au substrate does not have the 3-fold symmetry required by a model with all S atoms adsorbed at the Au hollow sites, and grazing incidence X-ray studies[7] suggest the presence of a disulfide bond, consistent with the sulfur atoms being adsorbed at both the Au hollow and bridge sites.

The focus of this work is to use ordered organic monolayers as model systems for the understanding of basic tribological issues. Previous studies of the mechanical properties of alkyl thiol monolayers on gold showed that a C_{22} acted as a "cushion" for Au substrates, even beyond the plastic limit of Au, when sufficiently "blunt" tips (radius of curvature >1000 Å) were used,[12] while with sharper tips (tip radius ∼700−1000 Å), a reversible transition from the thiol to the Au(111) was observed for loads of 250−300 nN.[13] This paper describes recent experiments performed on *n*-octadecanethiol (C_{18}) monolayers using tips with a radius of curvature between 100 and 300 Å. Under these conditions, the transition mentioned above is observed to take place at loads in the 10−40 nN range. A detailed study has been carried out to understand the nature of this transition. In particular, the tip height during the transition and frictional force through the transition have been measured, and the critical shear stress below the transition threshold has been estimated.

Experimental Section

Monolayer Preparation. Gold films were prepared by resistive evaporation onto freshly cleaved mica. The mica substrates were heated in vacuum to 250 °C for 2−3 h. The Au was deposited at a rate of 2−3 Å/s. After evaporation, the substrates were allowed to cool to <60 °C in vacuum, removed from the vacuum evaporator, and immediately immersed in a 1 mM solution of *n*-octadecanethiol in ethanol. The gold substrates were left in the solution at room temperature for at least 36 h, then rinsed with ethanol and dried in a N_2 stream. Octadecanethiol layers obtained in this way were observed by AFM to be stable in air for 4−6 weeks.

Instrumentation. AFM images were obtained with a home-built AFM system[14] using the optical lever deflection method[15] to simultaneously measure cantilever bending (normal force) and twisting (lateral force) and operating under ambient conditions. The *x* (fast) and *y* (slow) scan directions are perpendicular and parallel to the cantilever long axis. Commercially available gold-coated V-shaped silicon nitride cantilevers with nominal force constants of 0.5[16] and 0.58 N/m[17] were used.

Operating Modes. The normal deflection of the cantilever (and the externally applied load F_{ext}) is proportional to the difference between the light intensities measured by the top and bottom sectors of the photodiode, which we call the A−B signal. The cantilever twisting in the *x* direction, used for friction images, is proportional to the difference between the photocurrents detected by the left and right sectors of the photodiode, which we call the 1−2 signal. The two signals are decoupled by electronically adding or subtracting a fraction of the A−B signal from the 1−2 signal, so that the 1−2 voltage is constant during a force vs distance curve. Since the 1−2 signal is much smaller in magnitude than the A−B signal (25−30 times for the levers used in this study), it is important to take this precaution to avoid coupling of the topographic and friction data.

Data are acquired simultaneously for both signals in the forward (+*x*) and backward (−*x*) scan directions so that a set of four images is obtained for each scan. A +*x*/−*x* pair of scan lines of the frictional force images gives a "friction loop". Its

* Corresponding author. E-mail: salmeron@stm.lbl.gov.
† Permanent address: Department of Electronics, Glasgow University, Glasgow G12 8QQ, U.K.
‡ Permanent address: Fisica Aplicada, Facultad de Ciencias, Universidad Autonoma de Madrid, Campus de Cantoblanco, 28049 Madrid, Spain.
⊗ Abstract published in *Advance ACS Abstracts,* May 15, 1997.

S1089-5647(96)03807-2 CCC: $14.00

width is a measure of the frictional force.[18] For this work, the microscope was operated in two different modes, *topographic* and *variable load* mode. In the *topographic* or *constant deflection* mode, the A−B signal and the external load F_{ext} is kept constant by a feedback loop. Simultaneous images show the surface topography and variations in the lateral force. When the microscope is operated in the *variable load* mode, the feedback is disabled and the normal load is changed after each scan line by moving the sample up or down.[19] The *y* scan range is set to zero, and the A−B and the 1−2 signals are acquired simultaneously. The A−B data for each *x* scan line are averaged together and the result is plotted vs sample vertical displacement *Z*. The 1−2 image for the backward $-x$ direction is subtracted from that corresponding to the forward $+x$ direction, and then all the data points along each horizontal line are averaged together. The edges of the images corresponding to static friction effects are always excluded from the average. The 1−2 data so obtained are then plotted vs the A−B signal (load or F_{ext}). For the experiments reported here, most variable load mode curves were taken by first increasing and then decreasing the normal load. If friction is plotted vs the applied *Z* piezo voltage V_Z rather than lever deflection, the plot is significantly distorted by piezo hysteresis and creep, as shown in Figure 1.

Instrumental Calibration. In order to perform quantitative studies of friction, it is necessary to know the normal and lateral force constants of the cantilever, the sensitivity of the optical detection, and the shape of the tip.[20] Ideally this calibration is performed in *situ.* In this work, such calibrations were not available, so the quantitative data presented are based on estimated calibrations. The AFM tip radius *R* was estimated from the apparent width *w* of monatomic steps on Au(111) of height *h* by using the formula $R = w^2/2h$. Radii of curvature ranging from 100 to 300 Å were found for the tips used in the experiments described here. The piezo scanner lateral sensitivity was calibrated from lattice-resolution images of mica and Au-(111).

The normal force optical deflection sensitivity was determined from the slope of the A−B vs *Z* piezo voltage curves. Since the measured slope is affected by piezo hysteresis and creep, we averaged the slope of the approach and retract branches of a series of both normal, relatively fast, approach curves and the slower approach curves derived from variable load images. The small-signal *Z* piezo calibration was determined from monatomic step heights on Au(111) and from single-layer steps on mica, artificially generated by wearing the surface.[19] The lever displacement (A−B voltage) was converted to load using cantilever force constants estimated from a continuum elasticity model after measuring the levers critical dimensions by SEM.[20] In addition, the effect of the gold coating was taken into account using the method of Sader *et al.*[21] The lateral deflection sensitivity was assumed equal to the normal deflection sensitivity, and the force calibration was derived from an estimate of the relative deflection due to bending and twisting of the cantilever.[20] The values for forces and pressure quoted below are necessarily approximate due to the rough calibrations used here; however, we feel that they are probably correct within a factor of 2.

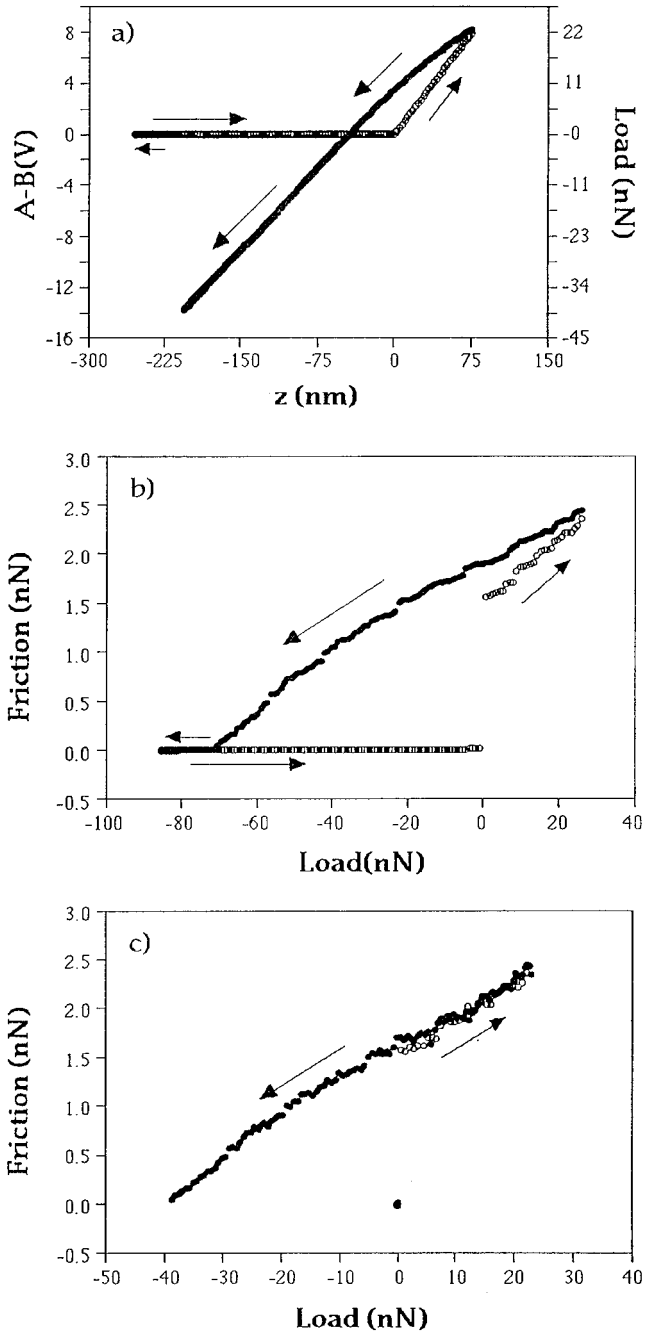

Figure 1. (a) Lever deflection signal vs piezo nominal displacement (applied piezo voltage V_Z) approach−retract curve; (b) friction vs nominal displacement; (c) friction vs A−B signal curves obtained on a mica surface. The values relative to approach and retract branches are shown as open and filled circles, respectively. For all curves, load is the externally applied force. Negative loads correspond to the tip being pulled off the surface. The hysteresis visible in (a) and (b) is due to the response of the piezoelectric transducer to the applied voltage. In (c), the hysteresis has disappeared. After the tip makes contact with the surface, the A−B signal is proportional to the piezo *Z* displacement, while the actual *Z* displacement is not proportional to the applied voltage V_Z due to piezo hysteresis and creep.

Results

Topographic Mode Images. Figure 2 has a topographic mode image showing that, at low external loads (0.5 nN, in this case), periodic AFM images are obtained. From this image and its corresponding image power spectrum, the lattice constant is 5.0 ± 0.3 Å. This corresponds well to the hexagonal ($\sqrt{3} \times \sqrt{3}$)R30° unit cell determined by diffraction studies[3,6,7] and is in close agreement with earlier AFM findings[10,13] for the periodicity of the C_{18} molecules.

Figure 2 shows that, when the load is increased and reaches a critical value, a new periodicity is observed in the AFM images. The lattice appears to be rotated 29° ± 1° with respect to the low load image (C_{18}) and the lattice constant is 2.9 ± 0.2 Å. Such a periodicity corresponds to the nearest-neighbor distance for the (1 × 1) structure of Au(111). Similar experiments performed on bare Au(111) with tips of similar

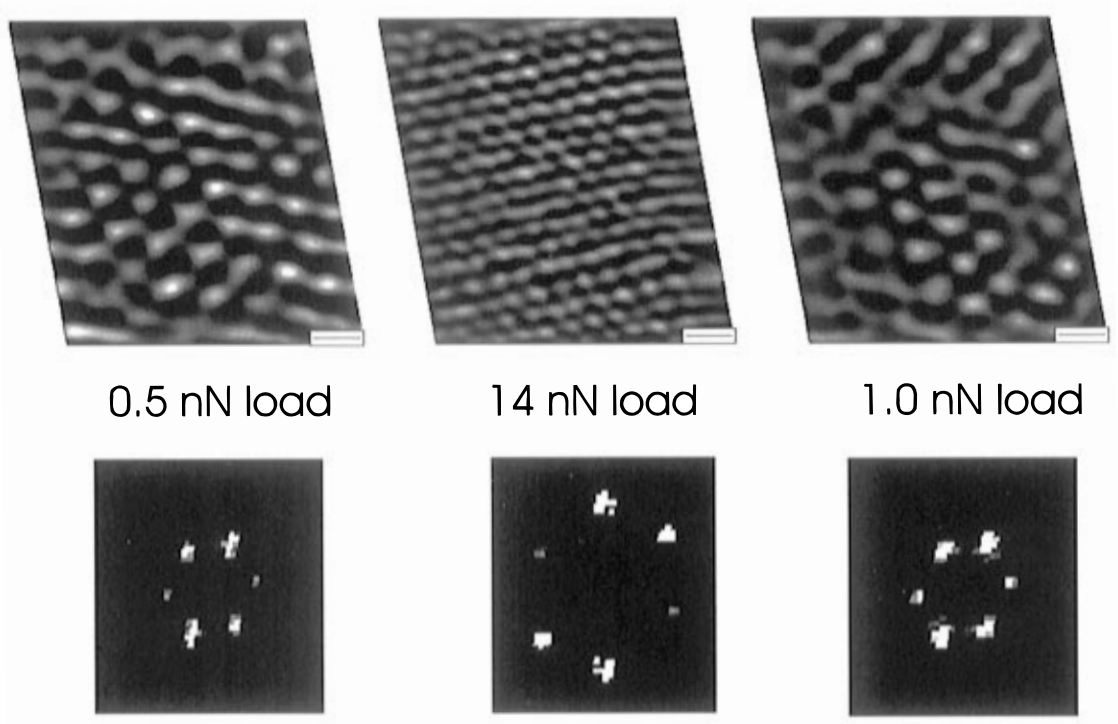

Figure 2. Frictional force images (and corresponding Fourier power spectra) obtained in topographic mode on a C_{18} thiol layer showing the reversible transition. The tip radius is ~150 Å. The scale bar is 5 Å. The initial AFM images taken at low load (0.5 nN) show the $(\sqrt{3} \times \sqrt{3})$R30° periodicity of the alkyl chains (5.0 Å lattice constant), consistent with diffraction studies. At a critical value of the load (14 nN), a transition to the 1 × 1 periodicity of Au is observed (2.9 Å lattice constant, rotated 30° with respect to the thiol lattice). Upon release of the pressure (back to 1 nN), the $(\sqrt{3} \times \sqrt{3})$R30° periodicity is recovered. The Fourier peaks in the final image after the transition were broadened compared to the initial image.

radius showed that the Au surface responds elastically to forces in this range, so the observed structural transition takes place below the elastic limit of gold.

As the load is decreased, the thiol periodicity is recovered and no visible permanent damage of the layer occurs.[13] In fact, large scale topographic images taken at low load after the transition did not reveal any holes or accumulation of material. However, as seen from Figure 2, molecular scale AFM images taken at low load after the transition are not as sharp as prior to it and the corresponding Fourier transform peaks are typically broadened by 30−60% and reduced in intensity by ~20−40%.

The transition from the $(\sqrt{3} \times \sqrt{3})$R30° to the (1 × 1) periodicity is not abrupt. In fact, several consecutive scans are required to reveal the Au(111) lattice (Figure 3), depending on the applied load and tip radius. An analysis of the intermediate scans shows that two lattices coexist in different parts of the images, as seen in the image Fourier power spectra.

To further investigate the nature of this transition, the following experiment was performed. An area was scanned at increasing load until the transition was observed to occur at ~23 nN, and then the tip was moved to a new area and several consecutive images were acquired at a load of ~17 nN. In this case, the thiol $(\sqrt{3} \times \sqrt{3})$R30° periodicity is observed after multiple scans (Figure 4). The spots in the corresponding Fourier images were broadened by ~60%, consistent with the real-space images.

After increasing the load to ~21 nN, the AFM images and corresponding Fourier images gradually became disordered. However, a 1 × 1 lattice was not observed even after multiple image scans. The Au 1 × 1 lattice was revealed only after increasing the load once again to ~23 nN. The critical load F_c required to initiate the structural transition is rather well-defined for a given tip.

Measurement of the Tip Height during the Transition. We believe that the structural transition occurs because the molecules are laterally and reversibly displaced from under the tip when the load exceeds the critical value. To check this, we monitored the vertical displacement *Z* of the tip during the transition. Under normal operating conditions, this is difficult to do since the thermal drift of our AFM in *Z* is ~0.1 Å/s. Furthermore, piezo creep effects cause changes in *Z* after a change in applied load. To minimize these effects, the microscope was set at the critical load of ~23 nN and left at the desired position on the sample for several hours to reach thermal equilibrium. These precautions reduced the drift rate by almost an order of magnitude. A small shift to a new area was then made before collecting data.

The *y* scanning range was set to zero so that the same horizontal *x* line was repeatedly scanned by the AFM tip while the feedback loop maintained the load constant. Topographic data were recorded for 24 consecutive images for a total time of 196.8 s. The *Z* data corresponding to each *x* scan line of the images were averaged together and plotted as a function of time (Figure 5). As can be seen in the plot, the value of *Z* is constant for the first ~20 s and then decreases monotonically until a first plateau is reached after ~80 s. At this point, the decrease in *Z* is ~18 Å. The tip remains constant at that height for ~45 s and then decreases again for an overall change in *Z* of 24 Å, after which no further changes were observed.

The thickness of the SAM, assuming an *all-trans* conformation of the alkyl chains and a tilt of 30° from the surface normal, is ~26 Å. The tip−surface separation decreases by approximately the monolayer thickness during the transition, which is consistent with a displacement of the molecules in the tip−surface gap.

Friction Measurements. Figure 6a shows a friction vs load curve obtained with a tip of radius ~200 Å. This result is

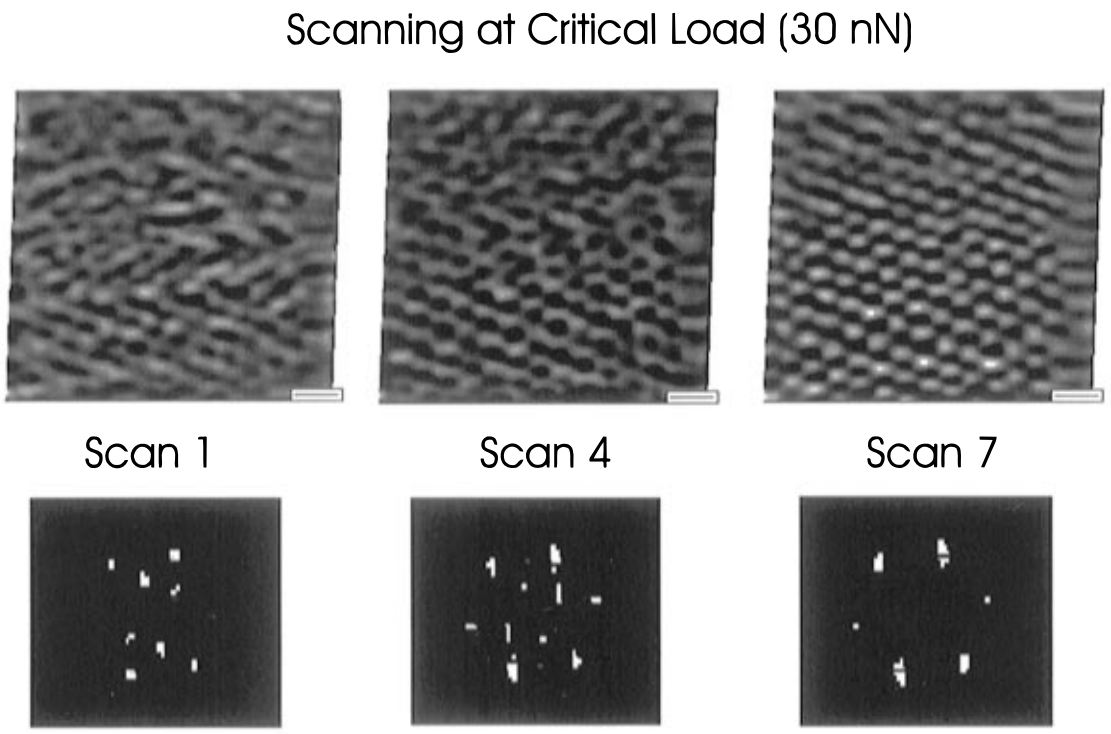

Figure 3. Evolution of frictional force images and corresponding Fourier power spectra obtained while scanning at the critical load (30 nN, in this experiment). The tip radius is ~230 Å. The first, fourth, and seventh scans of the series are shown. The scale bar is 5 Å. The $(\sqrt{3} \times \sqrt{3})$R30° to 1×1 transition is not abrupt. In fact, several scans (seven, in this particular experiment) are needed to reveal the Au lattice. At intermediate scans, both the thiol and the Au lattices are present in different regions of the AFM images. This is particularly clear in the Fourier plots, where the larger hexagon corresponds to the Au periodicity and the smaller one to the C_{18} overlayer.

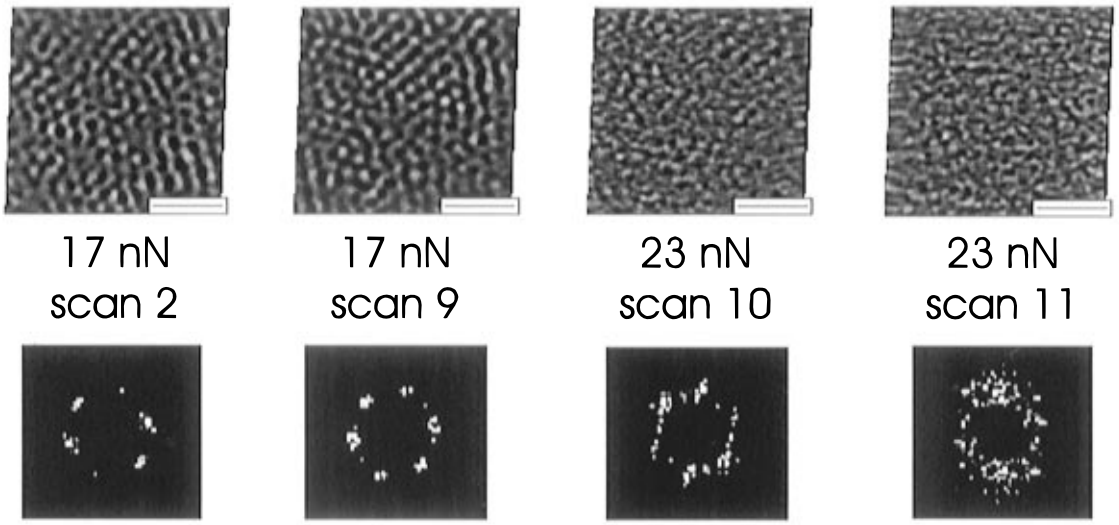

Figure 4. Part of a series of frictional force images and corresponding Fourier plots obtained while approaching the critical load (23 nN, in this experiment). Ten scans were made at 17 nN, and then the load was increased to 21 nN. The scale bar is 20 Å. At 6 nN below F_c, the AFM images reveal the $(\sqrt{3} \times \sqrt{3})$R30° periodicity. The fwhm's of the Fourier peaks were broadened by 30−60% between the second and ninth scans. This indicates changes in the degree of ordering in the chains. At 2 nN below F_c, the AFM images and corresponding Fourier peaks become gradually disordered.

typical of many experiments performed with sharp tips. The estimated lever force constant and normal to lateral deflection ratio are 0.62 N/m and 26, respectively. In this case, the critical transition load was 23 nN. The frictional force increases for loads up to the critical value until the onset of the transition, where a significant change is observed (marked by T in Figure 6a). Beyond this point, the frictional force either fluctuated with increasing load, as in Figure 6a, or decreased first and then stabilized (not shown). Similar behavior was observed as the load was decreased. A small amount of hysteresis was noted between the approach and retract branches.

Figure 6b shows the frictional force plotted as a function of load for a C_{18} thiol layer, as measured by a tip[17] with a radius of ~500 Å. The estimated normal force constant for this lever was 0.34 N/m,[22] and the bending to twisting sensitivity ratio was 28.[20] No transition could be observed with this tip for the range of loads investigated, which was typical for the experiments conducted with more blunt tips. As the tip radius is ~2.5 times larger than the case shown in Figure 6a, ~6 times more force or ~160 nN would be required to reach the pressure corresponding to the transition in Figure 6a. The required piezo extension of ~400 nm exceeded the range available with our

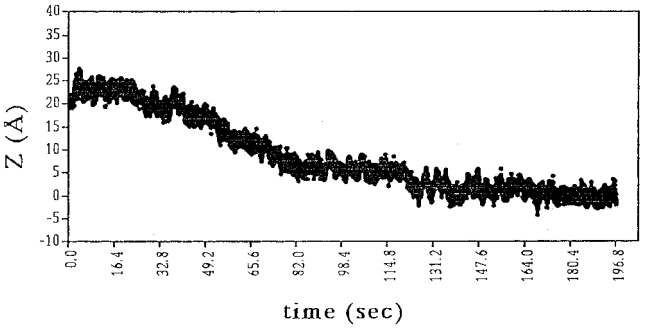

Figure 5. Vertical displacement of the tip Z measured as a function of time at the critical load (23 nN, in this experiment). The data correspond to 24 consecutive images where the tip was scanned in the x direction only, for a total time of 196.8 s. Each point in the graph represents the averaged Z value from a single line. The graph shows that the tip remains at a constant height with respect to the Au surface for ~20 s and then gradually approaches the Au surface. The decrease in Z between the initial and final positions is ~24 Å, *i.e.*, one C_{18} layer thickness. This is consistent with a displacement of the molecular layer during the transition.

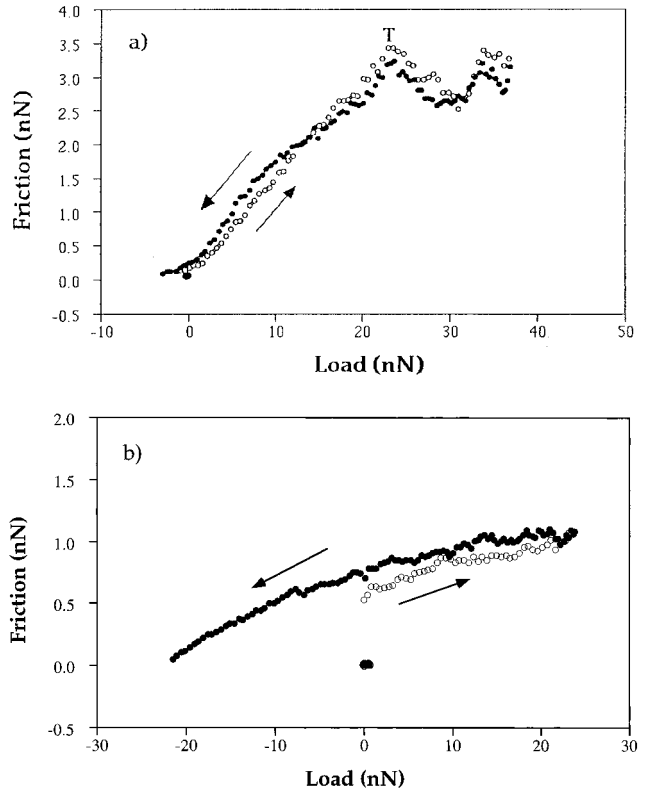

Figure 6. (a) Frictional forces measured through the transition from the $(\sqrt{3} \times \sqrt{3})$R30° to the 1×1 lattice. The critical load F_c is 23 nN in this experiment. Tip radius is ~200 Å. (b) Frictional forces measured with a blunter tip (tip radius ~500 Å) well below the critical load. Curve a shows that the transition is characterized by changes in the frictional force. No similar behavior is observed when blunter tips are used and the transition does not occur in this load range (b).

AFM. The shape of the curve in Figure 6b is generally similar to the pretransition region of Figure 6a. Some hysteresis can also be seen. The pull-off force in Figure 6b is larger than in Figure 6a, and the change in the friction slope just before pull-off in Figure 6a is not seen in Figure 6b.

The frictional forces shown in Figure 6a are ~3 times larger than those shown in Figure 6b for equivalent loads, even though the contact area at a given load for the sharp tip of Figure 6a should be a bit less than half that of the more blunt tip used for Figure 6b. This means that the friction per unit contact area at a given load is significantly greater for sharp tips than for blunt

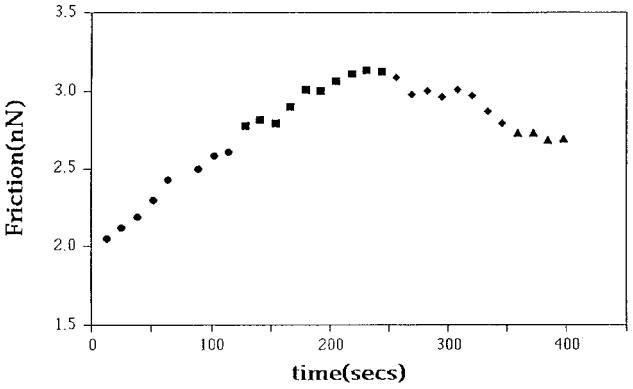

Figure 7. Frictional force measured for a number of sequential images at loads close to F_c (23 nN, in this case). Each point in the graph is the average frictional force measured in a complete image. Load: 17 nN (circles); 21 nN (squares); 23 nN (diamonds); 24.5 nN (triangles). Except for the points acquired at 24.5 nN, the frictional force is not constant at fixed values of the load. It increases for loads lower than F_c and decreases at F_c. This behavior is consistent with numerous defects being created in the chains, which provide modes through which energy can be dissipated (loads lower than F_c) and a decrease in the number of dissipative modes after the transition when the tip is in contact with the Au substrate.

tips. Although the numerical values are based on estimated force constants and approximate tip radii, we do not think that the numerical uncertainties can account for a 6-fold difference in lateral forces. Instead the shear force per unit area must increase with pressure. Pressure-dependent shear forces have been reported for organic Langmuir−Blodgett films.[23]

Figure 7 shows the frictional force measured in consecutive images for loads close to the critical load. Each point in the graph represents the average frictional force over an image. The friction increases during the first eight images at 17 nN (circles). During this time, the $(\sqrt{3} \times \sqrt{3})$R30° periodicity of the thiol layer is seen, but with increasingly broadened Fourier peaks. The next ten images at 21 nN (squares) were disordered. The transition occurs during the following eight images at 23 nN (diamonds) and the frictional force decreases as the 1×1 periodicity becomes visible. The friction is approximately constant during the final four images at 24.5 nN after the transition and the 1×1 periodicity is still visible.

Discussion

The first question in analyzing AFM images or friction data is the tip−surface contact area and its relation to the externally applied load. Tip−surface adhesion is usually important, as shown by the significant "pull-off" forces that are encountered in many AFM experiments. Since it was not possible to directly measure force and contact area with our AFM, a model had to be used to estimate the pressure applied by the AFM tip. Contact mechanics theories are available for this purpose.[24] One important issue is the role of adhesion. For the application of any model, the tip radius and the mechanical properties of the materials in contact (Young's modulus E and Poisson's ratio ν) must be known. The constants for Au ($E = 78.5$ GPa, $\nu = 0.42$) are taken from the literature.[25] A greater uncertainty exists for the silicon nitride lever and tip since the mechanical properties of CVD films are strongly affected by preparation conditions. Values of 140 GPa and 0.3 have been used here.[26]

The Hertz model describes the elastic deformation of solids in contact with no attractive interactions. The JKR theory includes the effect of local adhesive interactions in the contact proportional to the contact area, which causes additional elastic deformation of the solids and changes the contact geometry as

a function of load. There are also longer-range tip−surface forces that do not depend strongly on the contact area, such as the "capillary" force.[27] If the capillary force is the dominant interaction, which is often the case for AFM in ambient lab conditions, it is a reasonable approximation to use a "shifted Hertz model" with an effective load equal to the magnitude of the pull-off force added to the externally applied load. This is similar to the treatment of van der Waals forces in the DMT theory. The DMT and JKR models can be seen as limiting cases. Many authors have discussed the transition between these two cases.[28,29] The dimensionless parameter $\mu = [16R\gamma^2)/9K^2z_0^3)]^{1/3}$ is proposed as a way to choose a model, where R is tip radius, K is reduced elastic modulus, z_0 is a parameter representing the equilibrium separation of the surfaces in contact, usually taken as 0.2 nm, and γ is the contact adhesive energy per unit area. Large radii, strong adhesion, and soft materials characterize the JKR regime, represented by $\mu > 5$. Likewise, weak adhesion, hard materials, and small radii characterize the DMT regime, with $\mu < 0.1$.

If friction is proportional to contact area, then the JKR model makes the specific prediction that the friction at pull-off should be 40% of the friction at zero external load.[30] This is certainly not the case in the data of Figure 6b, and may not be in Figure 6a. From the pull-off force of Figure 6a, the interfacial energy for the tip−surface contact is ∼34 mJ/m^2, which is consistent with a van der Waals interaction. This yields a value for μ of 0.095, closer to the DMT regime. This discussion does not consider the modifications to the contact problem introduced by an elastic layer (the thiol molecules) on an elastic substrate (the gold film);[24] not only are the elastic properties of this layer difficult to characterize, but the stress/strain relation for the confined layer is probably not linear under the conditions of our experiments. In Figure 6b the pull-off force is much larger, and there seems to be a substantial capillary contribution in addition to the van der Waals term. For these reasons, we will use the shifted Hertz model to estimate contact areas and pressures.

The shape of the friction curve in Figure 6a is complex due to the thiol transition. The retract branch of the curve in Figure 6b is a good fit to the 2/3 power of effective load predicted by the Hertz model. From this, we can estimate the tip−sample interfacial shear strength to be 400 MPa.

($\sqrt{3} \times \sqrt{3}$)R30° to 1 × 1 Transition. The critical load F_c that induces the ($\sqrt{3} \times \sqrt{3}$)R30° to 1 × 1 structural transition clearly depends on the AFM tip radius. F_c was ∼14 nN for the ∼15 nm radius tip used in Figure 2, and ∼23 nN for the ∼20 nm tip in Figure 6a. If the shifted Hertz model is applied, a pressure of ∼2.3 GPa is obtained, with ∼30 (Figure 2) to ∼50 (Figure 6a) molecules involved in the contact. In general, for the tips used in this study, the critical load was found to be in the 10−40 nN range, or ∼0.5 nN/molecule. In earlier experiments, when blunter tips (tip radius 700−1000 Å) were used, F_c was ∼250−300 nN.[12] This is consistent with a critical load that scales with the square of the tip radius. In Figure 6b, the maximum effective load of ∼45 nN and tip radius ∼50 nm correspond to a mean pressure of ∼1.5 GPa, and the predicted critical load, which was not reached experimentally, would be ∼160 nN.

The energy associated with a single gauche defect (2.9 kJ/mol) is comparable to the thermal energy at room temperature (2.5 kJ/mol), so that little energy has to be spent to overcome this barrier.[31] In fact, nonlinear optical experiments on a variety of self-assembled and Langmuir−Blodgett films of long alkane molecules indicate that, even at pressures <80 MPa, much lower than those used in AFM experiments, terminal gauche defects are generated that tilt the CH_3 symmetric dipole of the terminal groups.[32] In these conditions, the AFM images show the long-range order of the alkyl chains. As the load and pressure increase and approach the critical value, more numerous defects are probably formed in the alkyl chains and the AFM images become gradually disordered. The binding energy of the sulfur head group to gold is ∼184 kJ/mol, and the packing energy of the C_{18} layer is ∼117 kJ/mol.[31] From the calculations of Siepmann and McDonald[33] we can estimate the "spring constant" of a single thiol molecule to be 3 N/m (E ∼36 GPa). At the transition load of ∼0.5 nN per molecule, the elastic energy is ∼25 kJ/mol. It seems plausible that the alkyl chains are being "melted" and disordered under the pressure applied by the AFM tip. Displacing the molecules under the tip will lead to a compression or increase in molecular density and strain energy in the region around the tip, which will be greater for blunt tips than for sharp ones. If the molecules were desorbed, then it seems likely that the transition would be irreversible. This model, analyzed in detail previously,[34] predicts a radius-dependent transition force, and that tips with radii > 100 nm will reach the plastic limit of gold before displacing the molecules.

Finally, when the pressure is released, the layer "heals itself" and the initial configuration is recovered almost entirely. The images taken at low load after displacement are normally less well-ordered. This is particularly apparent in the image Fourier transforms in which the spots have significantly broadened, indicating reduced domain size or imperfect packing in the molecular layer.

Our observations are in general agreement with molecular dynamic simulations of Tupper *et al.* that predict disordering of a C_{16} thiol under the pressure from a sharp tip or asperity[35] and with Monte Carlo calculations which predict a concentration of gauche defects at the methyl end of the hydrocarbon chains as increasingly high pressures are applied,[33] a result already found in our reported nonlinear optical studies.[32] We did not see any evidence for a change from hexagonal to oblique molecular packing under pressure, as was predicted in Tupper's simulation upon compression by a flat surface.

Friction Measurements. For pressures near the transition threshold, the thiol layer is not reducing friction, but rather increasing the work done in moving the tip across the surface. The tip−surface pressure is high enough to create defects in the thiol molecules. After the tip moves on, the molecules relax and energy is dissipated. The frictional force in Figure 6a near the transition is ∼3 nN for ∼50 molecules, so the work done in moving the tip would correspond to ∼0.2 eV/molecule, or 18 kJ/mol, if all the energy were dissipated in the thiol layer. The friction and energy dissipation increase in successive scans at the same load near the transition as the degree of disorder increases, as shown in Figure 7. A similar effect was seen in a study of friction vs chain length for self-assembled layers of alkylsilanes on mica, where friction was higher for shorter-chain, more disordered molecular layers than for the better-ordered, longer-chain overlayers.[36]

It is important to remember that, in most AFM friction experiments where load is varied, and in all the experiments presented here, the load is changed by decreasing the tip−sample distance to bend the cantilever. For instrumental reasons, the levers are mounted at an angle of 15−20° relative to the horizontal. A 10 nN change in force for a 0.62 N/m lever requires a 16 nm change in Z, and the lever tilt means that the tip will also move across the sample by ∼4 nm, *i.e.*, by a distance comparable to the tip−sample contact diameter, so unlike macroscopic friction experiments, the measurements are

not conducted in the same "track". This fact should be considered when interpreting friction data where surface modification is taking place, and may account for the fluctuations in friction observed above the transition load.

At the transition load, significant changes occur, as can be seen in Figures 6a and 7. While the details of frictional behavior above F_c vary from case to case, the frictional force always drops at the transition. Once enough molecules are displaced for the friction stick−slip to be in registry with the Au lattice, the friction decreases, even though the load and tip−surface contact area have increased.

Summary

AFM has been used to study the response of C_{18} alkyl thiol layers to pressures from few hundred MPa to a few GPa. AFM images show the long-range order of the alkyl chains, revealing the $(\sqrt{3} \times \sqrt{3})$R30° periodicity. The molecular packing lattice is resolved with relatively sharp (∼15 nm) and also with rather blunt (∼70 nm) tips at mean contact pressures up to ∼1.5 GPa; however, the c(4 × 2) superstructure is not observed. As pressure increases, the AFM images of the thiol lattice become increasingly disordered. At a well-defined critical pressure of ∼2.3 GPa, the Au(111) 1 × 1 lattice periodicity is observed while the tip−sample spacing decreases by approximately the thickness of the thiol layer. We believe that the thiol molecules are being reversibly squeezed out from under the tip while remaining in contact with the gold surface. When the pressure is reduced, the $(\sqrt{3} \times \sqrt{3})$R30° thiol lattice is again observed. Image Fourier transforms have broader spots, indicating that the domain size in the molecular overlayer may be reduced, but large-area, low-pressure AFM images show no signs of surface debris or of holes in the SAM layer. Friction first increases near the transition, and then drops above the critical pressure.

Acknowledgment. This work was supported by the Lawrence Berkeley National Laboratory through the Director, Office of Energy Research, Basic Energy Science, Materials Sciences Division of the U.S. Department of Energy under Contract DE-AC03-76SF00098. The authors thank Robert W. Carpick for helpful discussions on tribology and AFM calibration. A.L. acknowledges the partial financial support of the Commission of the European Communities.

References and Notes

(1) Nuzzo, R. G.; Allara, D. L. *J. Am. Chem. Soc.* **1983**, *105*, 4481.
(2) Porter, M. D.; Bright, T. B.; Allara, D. L.; Chidsey, C. E. D. *J. Am. Chem. Soc.* **1987**, *109*, 3559.
(3) Strong, L.; Whitesides, G. M. *Langmuir* **1988**, *4*, 546.
(4) Camillone, N.; Chidsey, C. E. D.; Liu, G.-y.; Scoles, G. *J. Chem. Phys.* **1993**, *98*, 3503.
(5) Nuzzo, R. G.; Dubois, L. H.; Allara, D. L. *J. Am. Chem. Soc.* **1990**, *112*, 558.
(6) Chidsey, C. E. D.; Liu, G.-y.; Rowntree, P.; Scoles, G. *J. Chem. Phys.* **1989**, *91*, 4421.
(7) Fenter, P.; Eisenberger, P.; Liang, K. S. *Phys. Rev. Lett.* **1993**, *70*, 2447. Fenter, P.; Eberhardt, A.; Eisenberger, P. *Science* **1994**, *266*, 1216.
(8) Poirier, G. E.; Tarlov, M. J. *Langmuir* **1994**, *10*, 2853. Poirier, G. E.; Tarlov, M. J.; Rushmeier, H. E. *Langmuir* **1994**, *10*, 3383.
(9) Anselmetti, D.; Baratoff, A.; Güntherodt, H.-J.; Delamarche, E.; Michel, B.; Gerber, Ch.; Kank, H.; Wolf, H.; Ringsdorf, H. *Europhys. Lett.* **1994**, *27*, 365.
(10) Alves, C. A.; Smith, E. L.; Porter, M. D. *J. Am. Chem. Soc.* **1992**, *114*, 1222. Pan, J.; Tao, N.; Lindsay, S. M. *Langmuir* **1993**, *9*, 1556. Liu, G.-y.; Salmeron, M. *Langmuir* **1994**, *10*, 367.
(11) Yeganeh, M. S.; Dougal, S. M.; Polizzotti, R. S.; Rabinowitz, P. *Phys. Rev. Lett.* **1995**, *74*, 1811.
(12) Salmeron, M.; Neubauer, G.; Folch, A.; Tomitori, M.; Ogletree, D. F.; Sautet, P. *Langmuir* **1993**, *9*, 3600.
(13) Liu, G.-y.; Salmeron, M. *Langmuir* **1994**, *10*, 367.
(14) Kolbe, W. F.; Ogletree, D. F.; Salmeron, M. *Ultramicroscopy* **1992**, *42*−44, 369.
(15) Marti, O.; Colchero, J.; Mlynek, J. *Nanotechnology* **1990**, *1*, 141. Meyer, G.; Amer, N. M. *Appl. Phys. Lett.* **1990**, *57*, 2089.
(16) Sharpened Microlevers; Park Scientific Instruments, Sunnyvale, CA.
(17) Pyramidal cantilevers; Digital Instruments, Santa Barbara, CA.
(18) Mate, C. M.; McClelland, G. M.; Elandsson, R.; Chiang, S. *Phys. Rev. Lett.* **1987**, *59*, 1942.
(19) Hu, J.; Xiao, X.-d.; Ogletree, D. F.; Salmeron, M. *Surf. Sci.* **1995**, *327*, 358.
(20) Ogletree, D. F.; Carpick, R. W.; Salmeron, M. *Rev. Sci. Instrum.* **1996**, *67*, 3298.
(21) Sader, J. E.; Larson, I.; Mulvaney, P.; White, L. R. *Rev. Sci. Instrum.* **1995**, *66*, 3789.
(22) Our estimated spring constant is less than the nominal value of 0.58 N/m provided by the manufacturer. However, the value reported in this paper is consistent with the experimentally determined values for levers of this type with the resonance frequency (52 kHz) observed in this study. See: Cleveland, J. P.; Manne, S.; Bocek, D.; Hansma, P. K. *Rev. Sci. Instrum.* **1993**, *64*, 403.
(23) Briscoe, B. J.; Evans, D. C. *Proc. R. Soc. London* **1982**, *A380*, 389.
(24) Johnson, K. L. *Contact Mechanics;* Cambridge University Press: New York, 1985.
(25) Goodfellow Catalog; Goodfellow Corporation, Malvern, PA.
(26) Zeigler, G. In *Preparation and Properties of Silicon Nitride Based Materials;* Bonnel, D. A., Tien, T. Y., Eds.; Trans Tech Publications: Zurich, 1989. The value for the Young's modulus was derived from the measured resonance frequency of the levers, with the assumption that the density ρ is 2.8 g/cm$^{3.}$
(27) Israelachvili, J. *Intermolecular and Surface Forces,* 2nd ed.; Academic Press: London, 1992; section 15.6. Fogden, A; White, L. R. *J. Colloid Interface Sci.* **1990**, *134*, 414.
(28) Maugis, D. J. *J. Colloid Interface Sci.* **1992**, *150*, 243.
(29) Carpick, R. W.; Agaït, N.; Ogletree, D. F.; Salmeron, M. *Langmuir* **1996**, *12*, 3334.
(30) Carpick, R. W., Agraït, N.; Ogletree, D. F.; Salmeron, M. *J. Vac. Sci. Technol. B* **1996**, *14*, 1289.
(31) Ulman, A. *Introduction to Ultrathin Organic Films: From Langmuir-Blodgett to Self-Assembly*; Academic Press: Boston, 1991.
(32) Du, Q.; Xiao, X.-d.; Charych, D.; Wolf, F.; Frantz, P.; Ogletree, D. F.; Shen, Y. R.; Salmeron, M. *Phys. Rev. B* **1995**, *51*, 7456.
(33) Siepmann, J. I.; McDonald, I. R. *Phys. Rev. Lett.* **1993**, *70*, 453.
(34) Salmeron, M.; Liu, G.-y.; Ogletree, D. F. In *Forces in Scanning Probe Methods*; Anselmetti, D., Meyer, E., Guntherodt, H.-J., Eds.; Kluwer Academic Publishers: Dordrecht, The Netherlands, 1995.
(35) Tupper, K. J.; Colton, R. J.; Brenner, D. W. *Langmuir* **1994**, *10*, 2041.
(36) Xiao, X.-d.; Liu, G.-y.; Charych, D. H.; Salmeron, M. *Langmuir* **1995**, *11*, 1600. Lio, A.; Charych, D. H.; Salmeron, M., to be published.